Metastability of Northern Hemisphere Teleconnection Modes

JAMES S. RISBEY, TERENCE J. O'KANE, AND DIDIER P. MONSELESAN

CSIRO Oceans and Atmosphere, Hobart, Tasmania, Australia

CHRISTIAN FRANZKE

Meteorologisches Institut, Universität Hamburg, Hamburg, Germany

ILLIA HORENKO

Institute of Computational Science, Universita della Svizzera Italiana, Lugano, Switzerland

(Manuscript received 30 January 2014, in final form 10 July 2014)

ABSTRACT

This study applies a finite-element, bounded-variation, vector autoregressive method to assess midtropospheric flow regimes characterized by regime switches between metastable states. The flow is assessed in reanalysis data from three different reanalysis sets assimilating surface data only; surface and upper-air data; and ocean, surface, and upper-air data. Results are generally consistent across the reanalyses and confirm the utility of surface-only reanalyses for capturing midtropospheric variability. The method is applied to a set of regional domains in the Northern Hemisphere and for the full-hemispheric domain. Composites of the metastable states for each region yield structures that are consistent with the well-documented teleconnection modes: the North Atlantic Oscillation in the Atlantic Ocean, the Pacific–North America pattern (PNA) in the Pacific Ocean, and Scandinavian blocking over Eurasia. The PNA mode includes a clear waveguide structure in midlatitudes. The Northern Hemisphere domain yields a state composite that reflects aspects of an annular mode (Arctic Oscillation), where the annular component in midlatitudes comprises a circumglobal waveguide. The Northern Hemisphere waveguide is characterized by wavenumber 5. Some of the nodes in this circumglobal waveguide manifest as part of regional dipole structures like the PNA. This situation contrasts with the Southern Hemisphere, where the circumglobal waveguide exhibits wavenumbers 3 and 5 and is monopolar. For each of the regions and modes examined, the annual time series of residence percent in each state displays prominent decadal variability and provides a clear means of identifying regimes of the major teleconnection modes.

1. Introduction

The background flow fields in the atmosphere are inherently unstable and support a wide range of modal structures, including large-scale, low-frequency modes (Frederiksen and Webster 1988). The Northern Hemisphere extratropical circulation is characterized by a number of temporally and spatially coherent large-scale structures or teleconnection patterns (Wallace and Gutzler 1981). The regional manifestations of these patterns include the North Atlantic Oscillation (NAO) (Wallace and Gutzler 1981; Hurrell 1995), the Pacific–North America pattern (PNA) (Wallace and Gutzler 1981), and a range of other structures. It has been argued that these regional structures may be manifestations of hemispheric-scale patterns, such as the Arctic Oscillation (AO) (Lorenz 1951; Thompson and Wallace 1998). Some of the patterns, such as the PNA, exhibit wavelike characteristics and may also be related to a circumglobal waveguide pattern (CWP) (Branstator 2002).

Various methods have been employed to describe these structures and to develop indices representing the current state of the structural mode. Representations of these structures are somewhat sensitive to the details of the methods used to construct them. However, the dominant regional modes, the NAO and PNA, correspond to the leading modes of spatial variability in winter midtropospheric height and are apparent using

Corresponding author address: James Risbey, CSIRO Oceans and Atmosphere, Castray Esp., Hobart, TAS 7000, Australia.
E-mail: james.risbey@csiro.au

DOI: 10.1175/JAS-D-14-0020.1

a range of different methods and variables (Hurrell and Deser 2009).

The persistent atmospheric structures are often called teleconnection patterns (Bjerknes 1969) because they are apparent in one-point correlation analysis methods, as documented by Wallace and Gutzler (1981), for instance. The teleconnection patterns have been extensively studied using eigenvector methods, such as EOFs or rotated principle component analysis (Barnston and Livezey 1987). The eigenvector methods generally give robust results for the leading modes (NAO and PNA), but successive modes are harder to interpret and explain progressively less variance (Hurrell and Deser 2009).

Hybrid methods that utilize regression coefficients with a base point to develop empirical orthogonal teleconnections have also been applied (Van den Dool et al. 2000). Franzke and Feldstein (2005) use a variant of this method to show that the PNA is driven primarily by interaction with climatological stationary eddies, whereas the NAO is driven primarily by transient eddy vorticity fluxes.

Branstator (2002) uses a combination of one-point correlation and the leading EOFs of 300-hPa streamfunction and nondivergent wind to highlight the CWP mode. Branstator (2002) notes that the jet stream waveguide provides meridional trapping of disturbances that can become zonally elongated and teleconnect around the hemisphere. This behavior is demonstrated by linearizing the barotropic vorticity equation about the mean 300-hPa streamfunction to recreate the dominant nodes of the CWP. The waveguide encompasses an NAO-like dipole structure in the North Atlantic.

Principal oscillation pattern (POP) methods have been employed to provide more dynamical insight into the major circulation modes. By fitting a tangent linear stochastic model to fluctuations about the mean state, the normal modes of the linearized system can be identified (von Storch et al. 1995). These modes correspond to the large-scale patterns of variability in the Northern Hemisphere revealed by earlier work. Frederiksen and Branstator (2001) use a linearized barotropic model to examine the growth of the normal modes in response to variations of the basic state through the annual cycle. They show that the growth rate of these modes is largest in winter and that the modes exhibit intraseasonal and longer-period variability.

The one-point correlation and eigenvector methods are linear and assume that the spatial structure of the dominant teleconnection modes is symmetric. A range of clustering methods has been applied to study of the modes that relax this assumption. The cluster methods typically use multivariate analysis (Hurrell and Deser 2009) or select multiple extrema in the phase space of the leading EOFs (Kimoto and Ghil 1993; Corti et al. 1999) to isolate recurrent patterns in the flow fields. Hurrell and Deser (2009) show asymmetries in structure between positive and negative phases of the NAO using a clustering method. Conventional clustering methods (k-means and mixture models) have been criticized because the number of clusters generated is dependent on the particulars of the algorithm and the period sampled (Christiansen 2007).

Since clustering methods select recurrent patterns but do not guarantee persistence of the resultant cluster patterns (Michelangeli et al. 1995), approaches have been developed fitting hidden Markov models to the flow field to generate clusters (Franzke et al. 2008, 2009). Where spectral gaps are identified in the eigenvalue spectrum of the Markov transition matrix, the corresponding states can be associated with persistent flow regimes or metastable states (Majda et al. 2006).

Clustering via hidden Markov model approaches has been used to identify persistent regimes and assess the metastable nature of these regimes in the Northern Hemisphere (Franzke et al. 2008, 2009). These studies show metastable states in a three-layer quasi-geostrophic model and in a barotropic model, respectively. Franzke et al. (2009) identify regimes in an atmospheric GCM corresponding to the AO and Pacific blocking. Franzke et al. (2011) apply hidden Markov model clustering to reanalysis fields for the North Atlantic domain, revealing two states corresponding to the positive and negative phases of the NAO, and a third state similar to the east Atlantic pattern (Wallace and Gutzler 1981; Barnston and Livezey 1987) or Atlantic ridge (Hurrell and Deser 2009). Franzke et al. (2011) also describe the role of wave breaking in setting transitions between North Atlantic regimes.

The above methods for identifying the teleconnection modes all assume statistical stationarity of the underlying flow fields. For example, the EOF method is a statistically stationary approach. EOFs are computed as the dominant eigenvectors of the time-independent covariance matrix of the data and are thereby time independent. The underlying assumption is that for all of the data at different times there is the same low-dimensional linear manifold that contains the highest fraction of the data variability. There are some nonstationary extensions of EOFs reported in the literature [e.g., the finite-element, bounded-variation, EOF method (FEM-BV-EOF) in Horenko (2010a)]. However, all of them imply deployment of some nonstationary tool on top of the standard stationary EOF approach.

In practice, the flow fields are not stationary. Finite-element, bounded-variation, vector autoregressive factor methods (FEM-BV-VARX) have been introduced to cope with nonstationarity (Horenko 2010a,b, 2011). Vector autoregressive models are fitted to the data to simultaneously estimate the flow regimes and the most likely transitions between them. The optimal number of regime states is determined using information theory. The method does not assume that the underlying processes are stationary or Markovian. It makes no assumptions about the structure of the data except that the flow switches between a finite number of states or regimes. The method is thus appropriate to regimes exhibiting metastability, as hypothesized for the atmosphere by Charney and DeVore (1979), for instance.

The FEM-BV-VARX approach is a general variational framework that reduces to k-means and hidden Markov approaches when more restrictive assumptions are made on the nature of the underlying data (Metzner et al. 2012). As special cases, the FEM-BV-VARX framework also contains such standard tools of stationary statistics as the multilinear regression and multivariate autoregressive models with (VARX), and without (VAR), external factors, allowing one to deploy these standard tools also beyond the usual stationarity assumption.

FEM-BV-VARX methods have been used in a regional domain in the Northern Hemisphere to identify blocking regimes over Europe (Horenko 2010b). O'Kane et al. (2013b) analyzed 500-hPa geopotential height reanalysis fields for the Southern Hemisphere using FEM-BV-VARX. They identified metastable states in the Southern Hemisphere circulation corresponding to a circumglobal three-wave blocking regime and a zonal southern annular mode (SAM) regime. The residence times in these states exhibited a trend away from the blocking state and toward the zonal state in the recent period. O'Kane et al. (2013a) used FEM-BV-VARX to analyze thermocline temperatures in a Southern Ocean domain of the Geophysical Fluid Dynamics Laboratory (GFDL) ocean GCM (OGCM). The OGCM exhibited metastable states featuring a decadal mode of variability in the South Pacific Ocean, with additional structure in the Southern Ocean storm track. The metastable states in the model ocean were amplified by atmospheric forcing of the OGCM.

This work extends the FEM-BV-VARX method to an analysis of the full hemispheric domain in the Northern Hemisphere atmosphere. A pertinent question is whether the FEM-BV-VARX method reveals the same persistent structures in the Northern Hemisphere as other approaches. Since FEM-BV-VARX assumes a switching process in the underlying fields, it provides a test of whether the canonical Northern Hemisphere teleconnection modes can be considered as metastable states. Further, since the method is not predicated on stationarity, it is legitimate to examine trend behavior in any of the identified states.

In the following sections, we describe the method used to apply FEM-BV-VARX to the Northern Hemisphere circulation. We show results for application of the method to the full hemispheric domain and to a set of sector domains designed to capture the major regional teleconnection patterns in the literature. In each case, we describe the spatial structure of the metastable states and relate time series of the residence behavior of the states to indices of the corresponding teleconnection patterns. The paper is structured around discussion of the major teleconnection patterns in each of the regions assessed.

2. Data and methods

The Northern Hemisphere circulation is represented in this study via daily 500-hPa geopotential heights, which provide a reasonable indication of midtropospheric flow in mid- and high latitudes. The seasonal cycle was removed from all datasets by subtracting from each daily value the climatological mean value over that day of the year, yielding daily anomalies of 500-hPa height. The FEM-BV-VARX analysis was applied to three different reanalysis datasets for the Northern Hemisphere: the Twentieth-Century Reanalysis, version 2 (20CR), spanning 1871–2011 (Compo et al. 2011); the National Centers for Environmental Prediction–National Center for Atmospheric Research (NCEP–NCAR) Reanalysis 1 (NNR1) spanning 1948–present (Kalnay et al. 1996); and the NCEP Climate Forecast System Reanalysis (CFSR) spanning 1979–2009 (Saha et al. 2010).

Part of the motivation for selecting three reanalysis sets is to examine whether the resultant metastable structures in the Northern Hemisphere are sensitive to the choice of reanalysis type. The 20CR provides a long record but assimilates surface data only. The NNR1 provides a multidecadal record with assimilation of surface and atmospheric data. The CFSR provides a short record but uses a coupled ocean–atmosphere model to do the reanalysis, allowing assimilation of some ocean data and some interaction between the ocean and atmosphere.

A set of experiments with the reanalysis sets spanning different periods were designed to test the influence of the different characteristics of the reanalyses. These experiments are shown in Table 1. The 20CR was run over the full period from 1871 and from 1948 only to test whether provision of a longer record improves the representation of metastable states (experiments 1 and 2). The shorter 20CR period (from 1948) corresponds to the period used for the standard NNR1 experiment and thus allows a direct comparison with NNR1 (experiments 2

TABLE 1. Periods used for the FEM-BV-VARX analysis for the given reanalysis.

Expt	Reanalysis	Period
1	20CR	1871–2009
2	20CR	1948–2009
3	NNR1	1948–2009
4	NNR1	1979–2009
5	CFSR	1979–2009

and 3). This comparison allows us to test whether the metastable structures can be captured using the cruder 20CR, which assimilates no upper-air data. The CFSR potentially allows us to test whether a coupled model improves the representation of metastable states. To allow a direct comparison with CFSR, the NNR1 was run over a second, shorter period of common years with CFSR (experiments 4 and 5).

In general, we found that the representation of metastable states is clearer with longer sampling and that the 20CR is capable of reproducing most features in the NNR1. Further, both the 20CR and NNR1 with many decades produce metastable states with a good resemblance to teleconnection patterns in the literature. The CFSR (1979–2009) and the shorter NNR1 period (1979–2009) are also able to reproduce the larger-scale metastable structures but not all smaller-scale features. The discussion of results will focus here on the longer period NNR1 and 20CR runs (the first three experiments in Table 1), but we show most experiments in each case.

We applied the FEM-BV-VARX analysis to the full Northern Hemisphere region and to a set of regional sectors in order to study the hemispheric modes and those only apparent in regional domains. The regions used are shown in Fig. 1 and denoted in Table 2, along with the modes of most relevance to each region.

Prior to the FEM-BV-VARX analysis, we reduced the dimensionality of the geopotential height anomaly data by extracting the leading 20 principal components (PCs), which is sufficient to characterize the flow (O'Kane et al. 2013b). The method is, however, not dependent on whether this reduction is performed (Metzner et al. 2012). A key advantage of reducing the dimensionality of the data is that it reduces the problem of ill-conditioning for short time series. Here, the patterns (EOFs) are discarded, and only the time-dependent PCs are retained in the analysis, since that is where the nonstationary components of the data reside.

The FEM-BV-VARX method (Horenko 2010a,b) relates the observed variable of interest x_t at a time $t \geq 0$ to the history of observations up to the time t and a time-dependent set of parameters θ_t. Formally, the relation is written as $x_t = f(x_{t-\tau}, \ldots, x_{t-m\tau})$, where $f(\cdot)$ is the model function, τ is the model time step, m is the time lag, and $m\tau \geq 0$ is the memory depth of the history dependence. FEM-BV-VARX approximates the dynamical processes governing x_t by a stochastic model of the form

$$x_t = \mu_t + A(t)\phi_1(x_{t-\tau}, \ldots, x_{t-m\tau}) + B(t)\phi_2(u_t) + C(t)\epsilon_t, \quad (1)$$

where $\mathbf{\Theta}(t) = [\mu(t), A(t), B(t), C(t)]$ is the vector of time-dependent model parameters with mean $\mu(t)$; ϕ_1 is, in general, a nonlinear function connecting present and past observations $(x_{t-\tau}, \ldots, x_{t-m\tau})$, but here we take it to be the linear autoregressive factor model. Also $\phi_2(u_t)$ is an external factor function, here set to 0, as we do not consider external factors in this study. The parameter $C(t)$ couples the Gaussian noise process ϵ_t to the

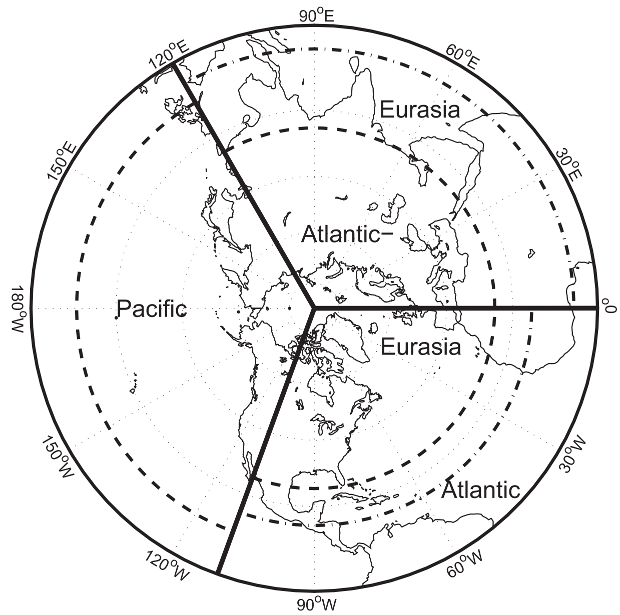

FIG. 1. Map of the Northern Hemisphere showing the regions used for the FEM-BV-VARX analysis. The entire Northern Hemisphere also forms one of the regions. The latitude and longitude domains for each region are given in Table 2.

TABLE 2. Regions used for the FEM-BV-VARX analysis. In each case, the latitude domain is 0°–90°N. The teleconnection modes characteristic of each region are listed in the last column.

Region	Lon	Relevant modes
Northern Hemisphere	0°–360°E	AO CWP waveguide
Eurasia	0°–120°E	Scandinavian pattern
Pacific	120°–250°E	PNA
Atlantic	250°–360°E	NAO
Atlantic–Eurasia	250°–120°E	TNH, WHW, and CWP

analyzed time series, which is modeled stochastically as an independent and identically distributed noise process (iid) with zero expectation. Time dependence of the model parameters $\boldsymbol{\Theta}(t)$ is induced by the influence of the noise and leads to regime transitions in many realistic systems (Horenko 2011).[1]

For a given number K of clusters and time lag m, the method minimizes the distance of the model trajectory (of model metric g) at each time t to one of the K model clusters. The model affiliation sequence

$$\boldsymbol{\Gamma}(t) = \gamma_1(t), \gamma_2(t), \ldots, \gamma_K(t) \qquad (2)$$

represents the probabilities of residing in each cluster state. The time-dependent vector $\boldsymbol{\Gamma}(t)$ contains the probabilities for an observation x_t at time t to be described by an output of a vector autoregressive external factor (VARX) model with constant (time independent) model parameters θ_i. The vector $\boldsymbol{\Gamma}(t)$ together with $\theta_1, \ldots, \theta_K$ are jointly obtained from a numerical optimization step as follows.

The method treats the clustering of nonstationary multidimensional data, $x_t \in R^d$, as a minimization problem:

$$L(\boldsymbol{\Theta}, \boldsymbol{\Gamma}) = \sum_{t=0}^{T} \sum_{i=1}^{K} \gamma_i(t) g(x_t u_t \theta_i) \rightarrow \min[\boldsymbol{\Gamma}(t), \boldsymbol{\Theta}], \qquad (3)$$

subject to convexity constraints $\sum_{i=1}^{K} \gamma_i(t) = 1, \forall t \in [0, T]$ and $\gamma_i(t) \geq 0, \forall t \in [0, T], \; i = 1, \ldots, K$. To select the proper order parameters for the VARX model and the optimal functional for external factors in Eq. (1), the lowest Akaike information criterion (AIC) value is chosen. Here AIC $= -2\log L_{\max} + 2M$, where $L_{\max}$ is the maximum log likelihood achievable by the model and M is the number of free parameters. The optimal model for the number of clusters K with a given persistency threshold is determined in this way as the best-fitting model with the fewest free parameters (Metzner et al. 2012).

From the model affiliation sequence $\Gamma(\mathrm{t})$, one can generate the Viterbi path $V(t)$, identifying the most likely cluster state i of the system at each time: $V(t) = \max_K [\gamma_i(t)]$. From the Viterbi path, one can construct composites by averaging x_t (500-hPa height anomalies) for each of the cluster states $i = 1, \ldots, K$ over all times when the system is in each state. For each of our domains, $K = 2$ cluster states were obtained, corresponding to the positive and negative phases of the dominant teleconnection modes. The composites show the spatial structure of each (metastable) cluster state. The Viterbi path $V(t)$ also allows a construction of the residence behavior of the system in switching between each cluster state. Composites for each metastable state were constructed for each of the seasons (December–February, March–May, June–August, and September–November) and over the full calendar year.

Composites were also generated by averaging over only those days in each cluster state where the residence time in the state was four consecutive days or more. This was done to test whether more directly persistent events have the same composite structure as the composites from the straight Viterbi paths. The results were broadly similar to those where this persistence test was not applied, so we show results without application of the persistence criterion.

The FEM-BV-VARX method embodies a form of sensitivity analysis in that an optimization is performed across all combinations of parameter values in Eq. (3). We do not a priori choose any specific value for memory depth m in Eq. (3) but set an upper bound and then loop through all possible choices (increments of a day) and employ the AIC to choose the optimal set of parameter values. Application of the AIC is equivalent to assuming that the scalar-valued squared model errors are χ^2 distributed and that the vector-valued FEM-BV-VARX model errors are Gaussian (i.e., dependent on the residuals having a lognormal distribution). This assumption has been tested using a nonparametric information-theoretic algorithm from Metzner et al. (2012). We found that, for all of the model errors, the optimal parametric family was indeed the lognormal distribution.

The following sections describe the FEM-BV-VARX metastable states for each of the domains examined. For composite plots of the metastable states, we show polar or cylindrical projections depending on the region. For regions where the dominant mode has nodes at high latitudes, the structure is usually clearer in a polar projection, whereas some modes display midlatitude waveguides that are clearer in cylindrical space.

Note that the numbering of a cluster state as 1 or 2 is arbitrary such that state 1 in one reanalysis may be equivalent to state 2 in another. To ease comparison of states between reanalyses, we display them in the

[1] In fact, it is well known that stochastic forcing of the large scales can induce low-frequency variability associated with regime behavior. For example, Bouchet and Simonnet (2009) developed a model with no background gradient of potential vorticity (no topography or meridional temperature gradients) and therefore no planetary or topographic Rossby waves, which, when subjected to weak stochastic forcing representative of unresolved processes, exhibits irregular low-frequency zonal-dipolar regime transitions. Here we parameterize unresolved atmospheric scales in the reanalyzed atmospheric 500-hPa height time series data as $C(t)\epsilon_t$. Such unresolved scales are mostly related to convective processes, which are inherently stochastic, so this approach seems sensible.

following so that the same phase is in the same column for each reanalysis experiment.

3. Cluster composite structures

a. Atlantic

The dominant teleconnection pattern in the Atlantic region is the NAO. The NAO emerges clearly in the FEM-BV-VARX analysis of the Atlantic region in all the reanalysis datasets. The annual mean composites for height anomalies in the two NAO states are shown in Fig. 2. Each of the reanalysis sets (20CR 1871–2009; 20CR 1948–2009; NNR1 1948–2009; and CFSR 1979–2009) shows a node near Greenland cradled by a broad node spanning the Atlantic in midlatitudes. This structure is nearly symmetrical across the two cluster states (NAO±) in 20CR 1871–2009 (Fig. 2a), NNR1 1948–2009 (Fig. 2c), and CFSR 1979–2009 (Fig. 2d), in contrast to the asymmetries in NAO cluster states in Hurrell and Deser (2009). However, the FEM-BV-VARX states are spatially "noisier" and less symmetrical in 20CR 1948–2009 (Fig. 2b). The asymmetry and noise in the 20CR 1948–2009 experiment are indications that the states are undersampled, relative to the longer 20CR experiment. The NAO state is better represented in NNR1 than 20CR with equivalent years (1948–2009), but with a longer record from 1871–2009, the 20CR produces an NAO structure very similar to that in NNR1.

The NAO states are present in composites over each of the four seasons in the FEM-BV-VARX analysis (not shown). The amplitude of the NAO pattern is weaker in summer but still evident, and there is a small latitudinal migration of the nodes with season consistent with Barnston and Livezey (1987).

b. Pacific

In the North Pacific region, the PNA emerges as the dominant mode of variability in studies using a range of different methods (Barnston and Livezey 1987). The PNA exhibits a pressure "seesaw" in the Aleutian low (Wallace and Gutzler 1981) and a wavelike structure across the North Pacific (Barnston and Livezey 1987). The wavelength of the Rossby wave structure varies seasonally in accordance with seasonal variation in speed of the westerlies (Barnston and Livezey 1987).

The pressure seesaw and waveguide aspects of the PNA are readily apparent in the FEM-BV-VARX cluster states for the Pacific region in Fig. 3. The Aleutian low seesaw is most prominent in Fig. 3a for 20CR 1871–2009. For the shorter 20CR 1948–2009 (Fig. 3b), the Pacific waveguide is more prominent than in the longer reanalysis, which appears to smooth the teleconnection pattern in this case. The structure of the Aleutian low and waveguide in 20CR 1948–2009 is well mirrored in the NNR1 spanning the same period (Fig. 3c). The shorter-period reanalyses (NNR1 1979–2009 and CFSR in Figs. 3d and 3e, respectively) also yield an Aleutian low node and waveguide but with an accentuation of the waveguide.

The FEM-BV-VARX cluster states for the four seasons (not shown) display the same basic structures as the annual mean in Fig. 3. The main change between the seasons is a prominent shortening of wavelength of the waveguide feature from winter to summer, consistent with the results of Barnston and Livezey (1987).

c. Eurasia

Teleconnection patterns in the Eurasia region feature a prominent wave train spanning Europe and Asia. This pattern was originally called the Eurasian pattern in Wallace and Gutzler (1981). Barnston and Livezey (1987) later distinguished between a type-1 and type-2 variant of this pattern, and the former of these is denoted the Scandinavia pattern (SCAND) by the National Oceanic and Atmospheric Administration (NOAA)'s Climate Prediction Center (Bueh and Nakamura 2007). A prominent node of this pattern sits over Scandinavia and reflects Scandinavian blocks in the positive phase of the pattern.

The canonical Scandinavian pattern is captured by the FEM-BV-VARX clustering for each of the reanalysis experiments in Fig. 4. The Scandinavian node is dominant and similarly located in each reanalysis cluster. For all but the 20CR 1948–2009 experiment (Fig. 4b), the annual composites are highly symmetrical for the positive and negative cluster states.

The seasonal composites for the Scandinavian pattern states (not shown) display two major differences between winter and summer. One difference is a weakening of the amplitude of the nodes in summer. The other difference is the presence of a North Pacific node of the pattern in winter. This node is only weakly present in the annual composites in Fig. 4. This result is consistent with the findings of Bueh and Nakamura (2007), who note that "remote influence from the North Pacific via Rossby wave propagation is apparent only in January and February."

d. Atlantic–Eurasia

The Atlantic–Eurasia region analyzed here (Fig. 1) covers nearly two-thirds of the hemisphere and thus encompasses regions displaying a range of different modes of variability. The annual mean composites for the FEM-BV-VARX analysis for this region for each reanalysis experiment are shown in Fig. 5. The dominant feature of the metastable structures is a waveguide

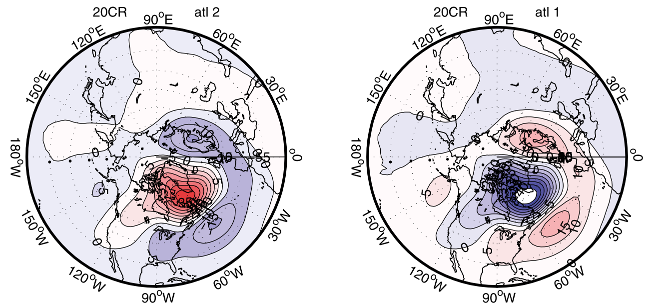

(a) 20CR 1871–2009

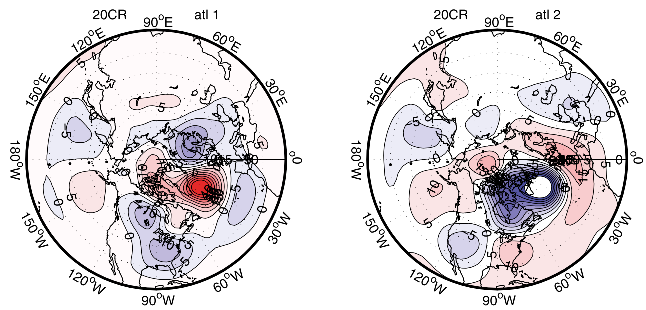

(b) 20CR 1948–2009

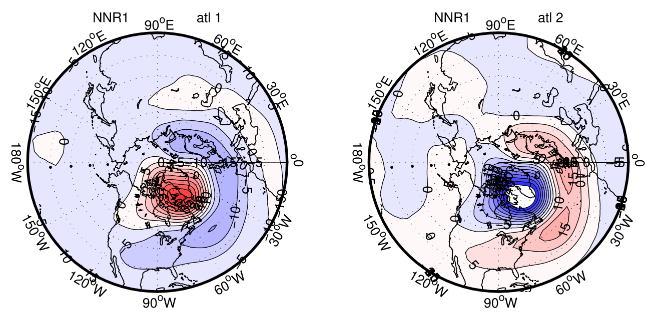

(c) NNR1 1948–2009

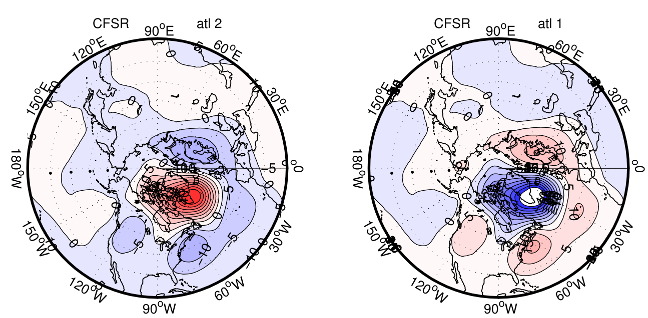

(d) CFSR 1979–2009

FIG. 2. FEM-BV-VARX composites of 500-hPa geopotential height anomalies for cluster states 1 and 2 for the Atlantic region. The reanalysis set and period are denoted in the figure. The composites include all months of the year.

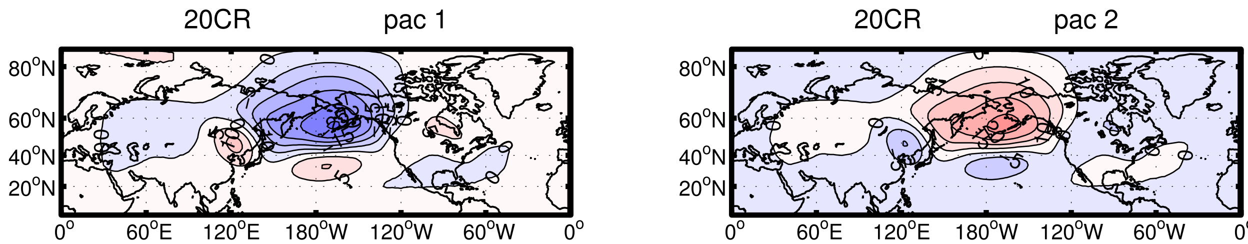

(a) 20CR 1871–2009

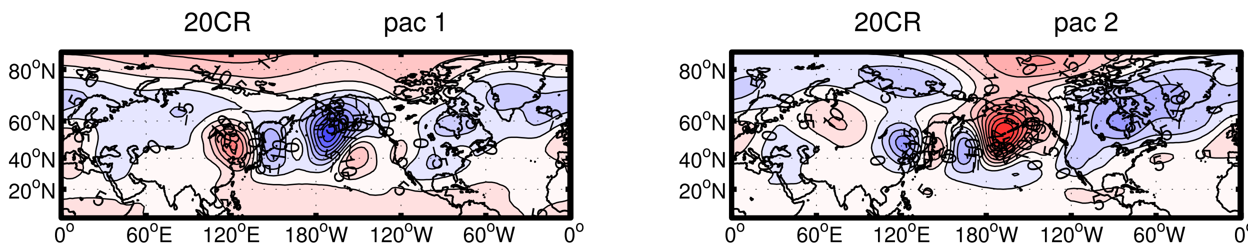

(b) 20CR 1948–2009

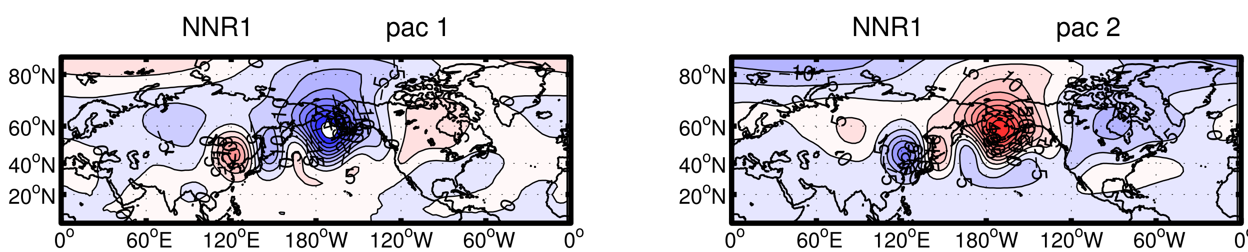

(c) NNR1 1948–2009

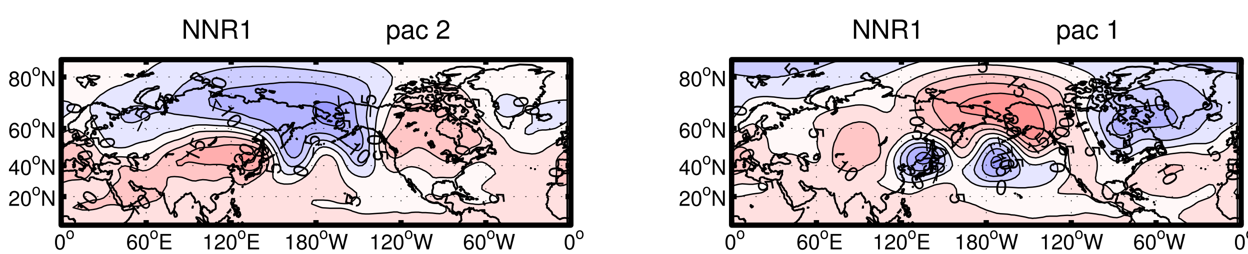

(d) NNR1 1979–2009

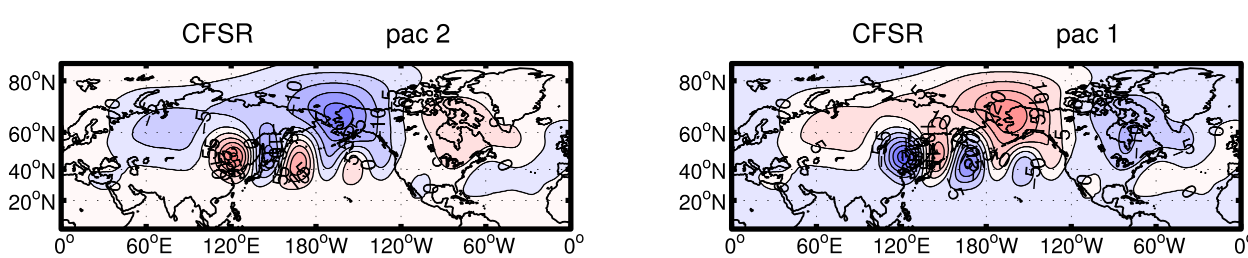

(e) CFSR 1979–2009

FIG. 3. FEM-BV-VARX composites of 500-hPa geopotential height anomalies for cluster states 1 and 2 for the Pacific region. The reanalysis set and period are denoted in the figure. The composites include all months of the year.

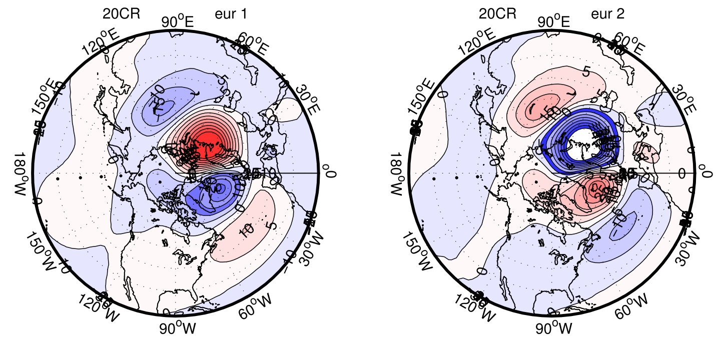

(a) 20CR 1871–2009

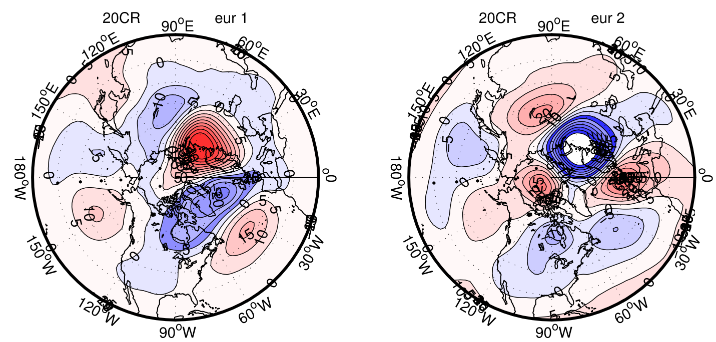

(b) 20CR 1948–2009

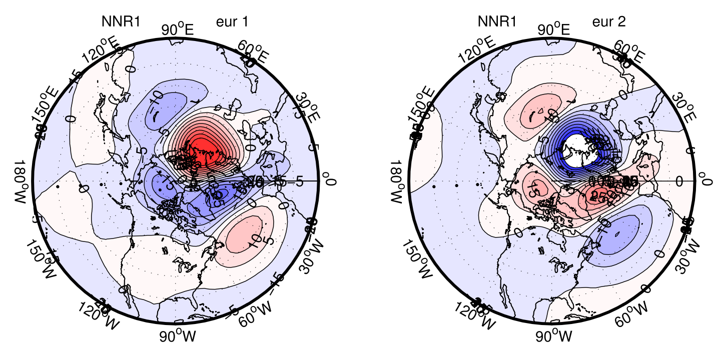

(c) NNR1 1948–2009

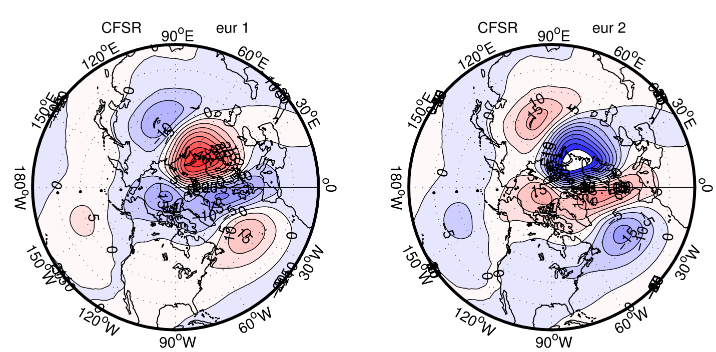

(d) CFSR 1979–2009

FIG. 4. As in Fig. 2, but for the Eurasia region.

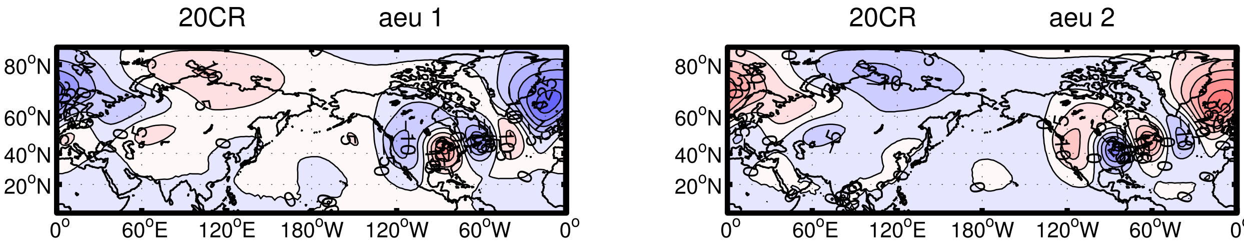

(a) 20CR 1871–2009

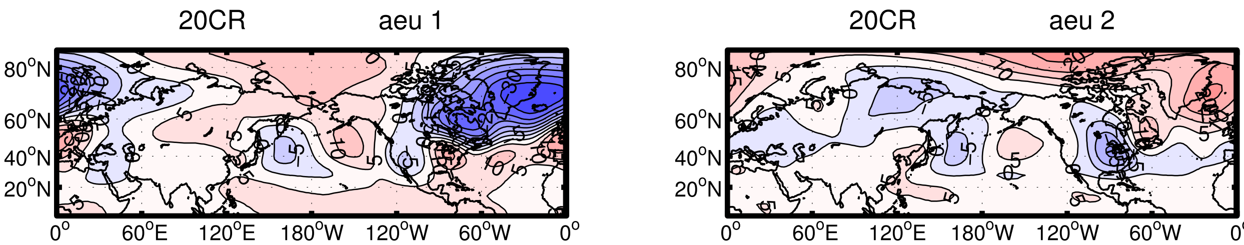

(b) 20CR 1948–2009

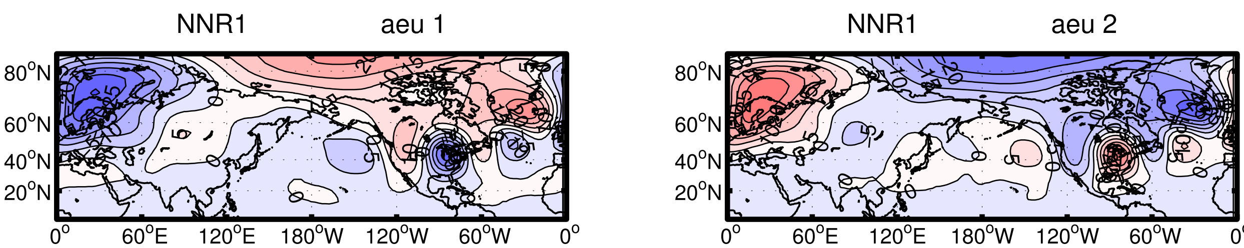

(c) NNR1 1948–2009

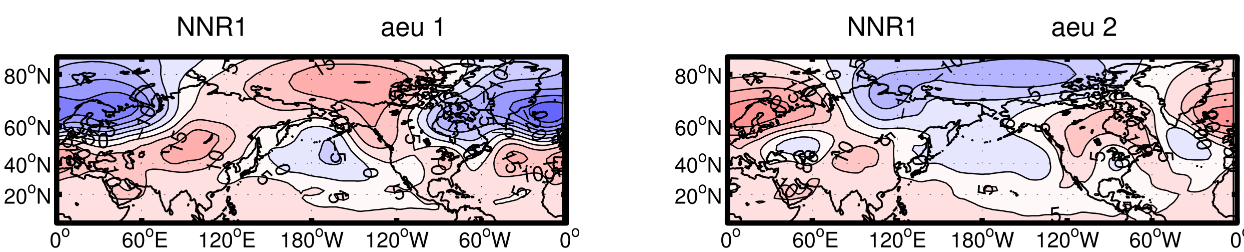

(d) NNR1 1979–2009

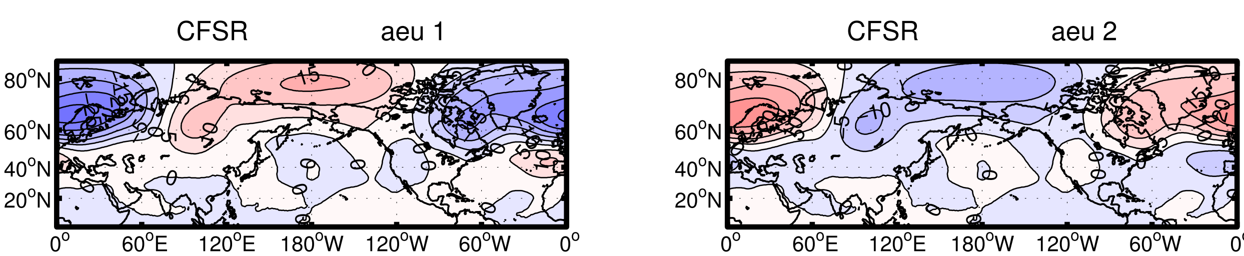

(e) CFSR 1979–2009

FIG. 5. As in Fig. 3, but for the Atlantic–Eurasia region.

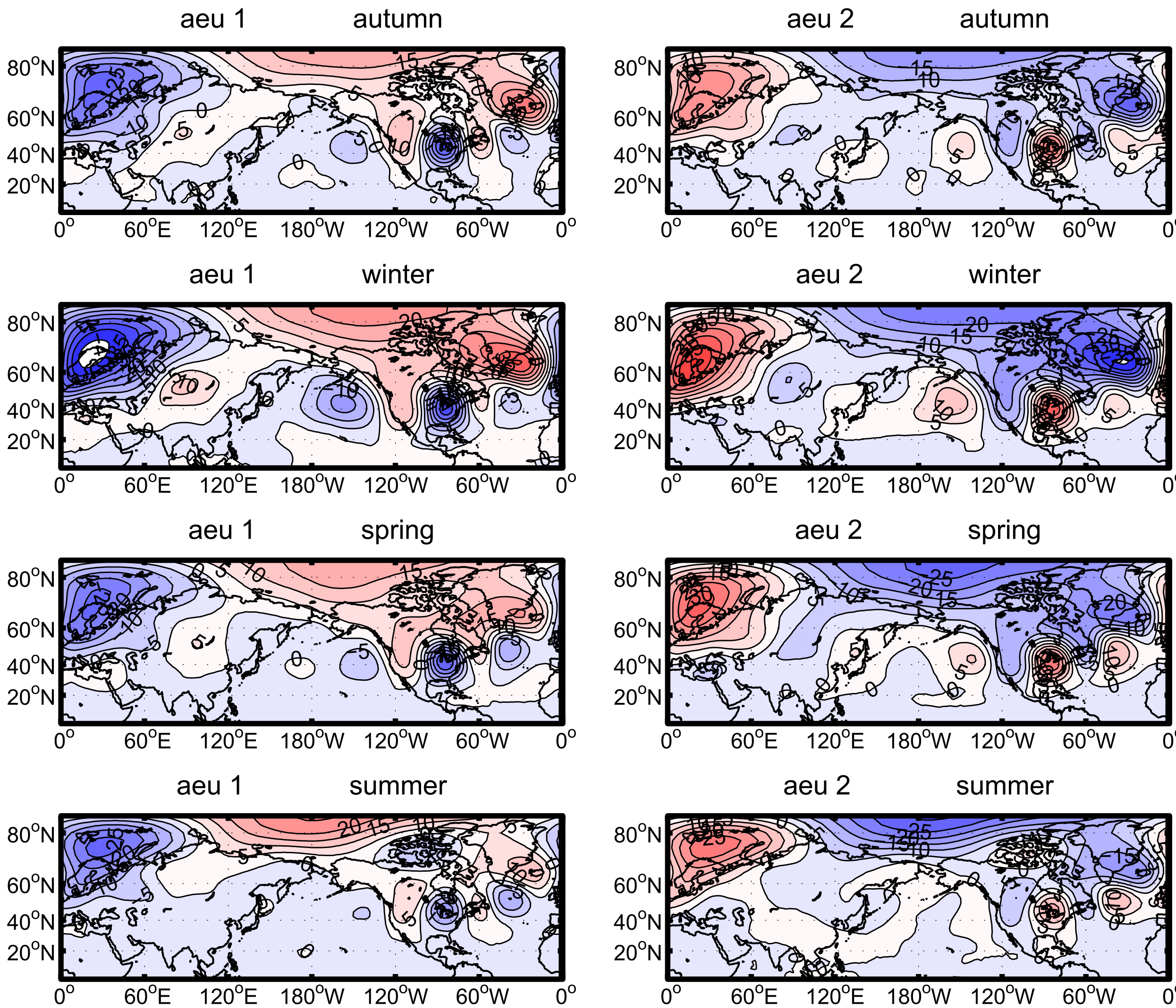

FIG. 6. FEM-BV-VARX composites of 500-hPa geopotential height anomalies for cluster states 1 and 2 for each season for the Atlantic–Eurasia region for the NNR1 1948–2009 experiment.

across North America and the North Atlantic into the Europe region. We will refer to this as the Western Hemisphere waveguide (WHW), as it is mostly evident in western longitudes. This waveguide bears some similarity to the tropical Northern Hemisphere (TNH) pattern described by Mo and Livezey (1986) and Barnston and Livezey (1987). The resemblance between the patterns is clearer when plotted in the polar projections used in those studies (not shown). We prefer to show the cylindrical projection here to emphasize the wavelike characteristics of this metastable mode.

The WHW is apparent in all the reanalysis experiments in Fig. 5, but is less well resolved in the NNR1 1979–2009 and CFSR 1979–2009 experiments. The larger scale features of the cluster composites are similar in these experiments to the other (longer) reanalysis experiments, but the smaller-scale wave train is less apparent over the shorter period.

The seasonal variation of the composite clusters for the Atlantic–Eurasia region is illustrated with the NNR1 1948–2009 experiment in Fig. 6. The waveguide structure persists through each of the seasons but is weaker in amplitude in summer. It is also apparent in the seasonal figures that the waveguide is not confined just to the Western Hemisphere longitudes. Rather, it extends globally, with weaker nodes spanning the North Pacific region. As such, this mode reflects Branstator's (2002) CWP, albeit with accentuation in western longitudes.

e. Northern Hemisphere

The leading mode of variability for the Northern Hemisphere domain in winter is a zonally symmetric pressure seesaw in mid- and high latitudes (Lorenz 1951; Wallace and Gutzler 1981). The surface signature of this pattern is the AO, which exhibits variability on intraseasonal, interannual, and longer time scales (Thompson and Wallace 1998). When using streamfunction (rather than geopotential) as a measure of circulation variability, Branstator (2002) highlighted the CWP mode, which is prominent in the jet stream waveguide regions of Northern Hemisphere middle latitudes.

The FEM-BV-VARX cluster states for the Northern Hemisphere domain are shown in Fig. 7. The cluster states exhibit both of the above characteristics (AO and CWP). The clusters show a midlatitude waveguide spanning much of the hemisphere that corresponds to the CWP mode (Figs. 7a–c). The CWP displays a wave-5 pattern in the jet stream waveguide, with a high latitude node over northern Europe, consistent with Branstator (2002).

The CWP wave train is embedded in the midlatitude portion of the AO, as becomes further apparent by showing the Northern Hemisphere cluster composites in polar perspective (Fig. 8). The zonally symmetric seesaw (AO) is evident in the cluster states in Fig. 8, with two key differences from the canonical form in Thompson and Wallace (1998). In the cluster composite, the center of the AO annulus (Arctic node) is not centered on the pole but is displaced from the pole. Further, the midlatitude ring of the AO pattern is not zonally uniform but, rather, contains zonal asymmetries because of the presence of the CWP. The CWP is less apparent in annual composites for the two shorter reanalyses (NNR1 1979–2009 and CFSR 1979–2009; Figs. 7d,e), though the waveguide is evident in seasonal composites for these reanalysis experiments (not shown).

The seasonal variation of the FEM-BV-VARX clusters for the Northern Hemisphere region is illustrated with the 20CR 1871–2009 experiment in Fig. 9. The CWP waveguide is evident in all seasons but has weakest amplitude in summer. The waveguide migrates seasonally with latitude, consistent with the seasonal migration of the major jet streams. The persistence of the waveguide through summer has been linked in part to thermal forcing from the Indian summer monsoon (Ding et al. 2011). The spatial location of the waveguide nodes downstream from central Asia appears consistent with this role.

4. Teleconnection indices

The FEM-BV-VARX composite cluster states identified in the previous section display similar patterns to the canonical modes of atmospheric teleconnectivity identified using alternative methods. Indices have been developed in the literature to describe the atmosphere's position or state in each of the teleconnection modes and to describe the time evolution of these states. In this section, we compare indices of the FEM-BV-VARX cluster states with indices of the teleconnection features from the literature as appropriate to each regional domain examined.

In the case of FEM-BV-VARX, the cluster index is simply given by the sequence of cluster state affiliations in the Viterbi path. Since two cluster states were obtained in each regional analysis here, the Viterbi path signifies at each time whether the system is preferentially in state 1 or state 2. For the daily resolution reanalysis data, the daily index is simply state 1 or state 2. We also generated cluster indices at monthly and annual resolution by calculating the percentage of days in each month and year in each of the two states and denote this as the residence percent.

The conventional teleconnection indices in the literature are continuous rather than discrete and usually correspond to a measure of the teleconnection pattern amplitude, such as principal components. For each region here, we use the index data from the NOAA/NCEP teleconnection archive (http://www.cpc.ncep.noaa.gov/data/teledoc/telecontents.shtml). The indices in the NOAA/NCEP archive are defined at daily resolution (AO, NAO, and PNA) and monthly resolution (SCAND).

For ease of comparison and to highlight longer-period variability, we show series of the FEM-BV-VARX and NOAA/NCEP teleconnection indices at annual resolution in Fig. 10. For FEM-BV-VARX, we show results from the NNR1 1948–2009 experiment, except for the Eurasian region, where we show 20CR 1948–2009, because the NNR1 experiment has a start-up trend of cluster state in that region. For the large-scale, robust, NAO (Atlantic) and PNA (Pacific) modes, there is little difference in the FEM-BV-VARX residence percent series produced from the 20CR or NNR1. For the Scandinavian blocking mode (Eurasia), the differences between the series from the two reanalyses are also small. For the CWP–AO mode (Northern Hemisphere) the cluster-state time series produced from the 20CR and NNR1 are not identical, and there is some sensitivity to choice of reanalysis set. The following sections describe the time series behavior of cluster states in each region.

a. Atlantic

For the Atlantic region, the FEM-BV-VARX cluster state series are plotted with the NOAA/NCEP NAO series in Fig. 10a. The NAO is highly correlated with the cluster series ($r = \pm 0.76$). This is not surprising, given that the cluster pattern in Fig. 2 so closely resembles the

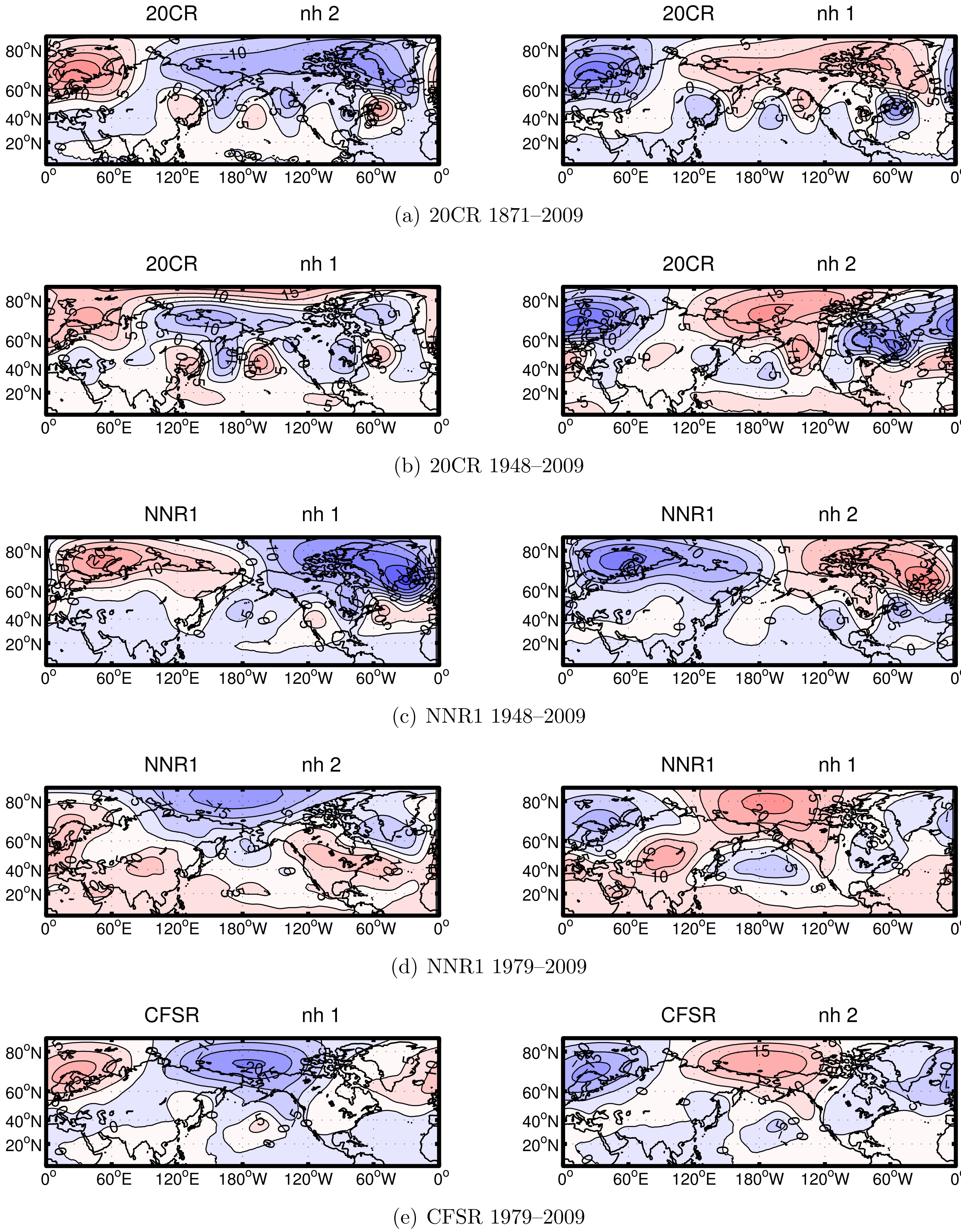

FIG. 7. As in Fig. 3, but for the Northern Hemisphere.

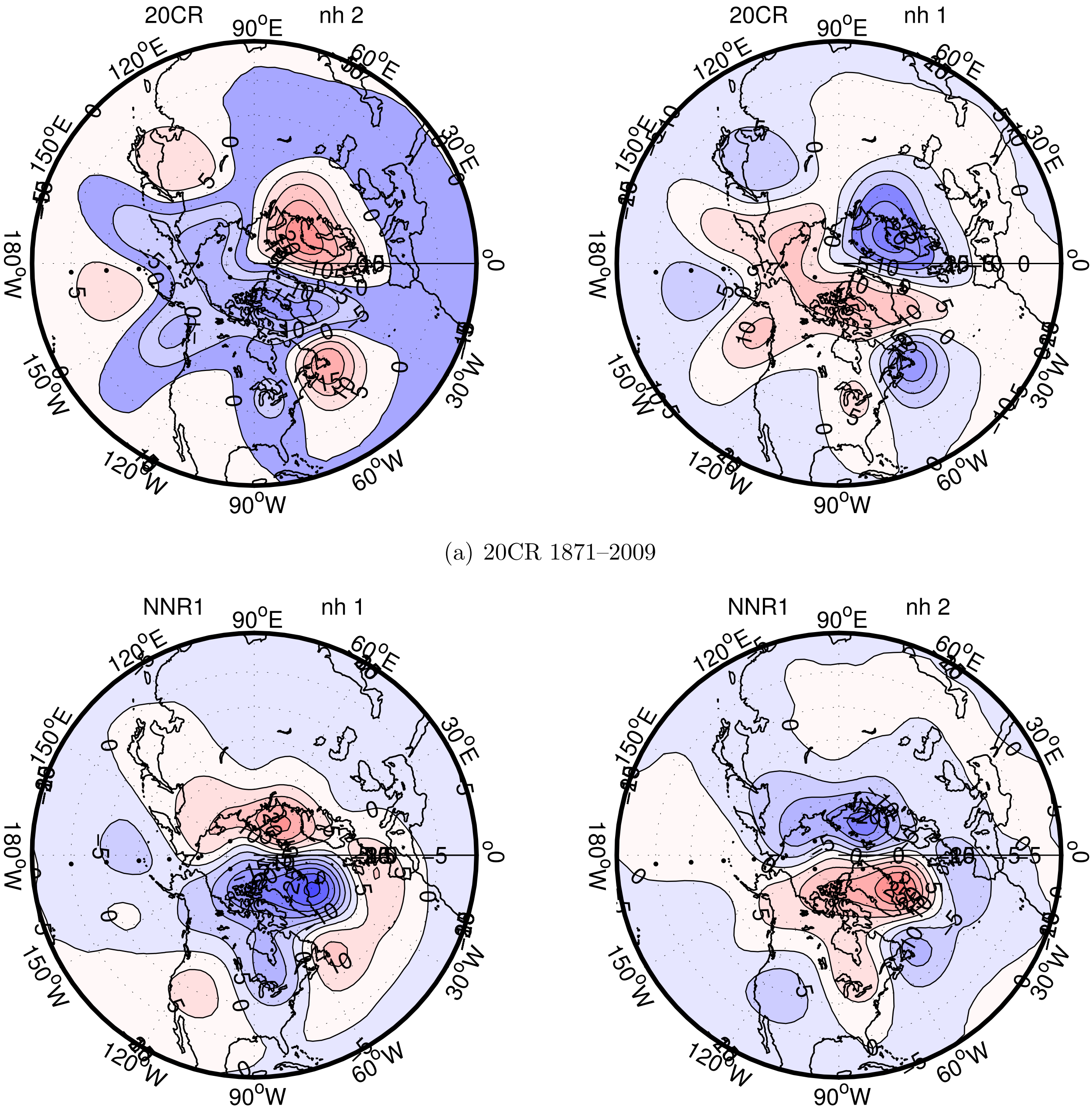

(a) 20CR 1871–2009

(b) NNR1 1948–2009

FIG. 8. As in Fig. 7, but with a polar projection and for just the 20CR 1871–2009 and NNR1 1948–2009 experiments.

canonical NAO pattern. The cluster series exhibits multidecadal variability with sustained periods of a decade or two where one state is more dominant than the other. This is consistent with observed multidecadal variability in the NAO (Hurrell 1995).

Indeed, the multidecadal regimes documented in the NAO are clearly revealed in the FEM-BV-VARX cluster series. Cluster state 1 (atl 1) corresponds to positive height anomalies at high latitude (Fig. 2c, left panel) and thus to NAO−. Cluster state 1 dominates cluster state 2 (atl 2) (NAO+) between 1950 and about 1980, corresponding to the period of observed NAO− dominance (Hurrell 1995; Visbeck et al. 2001). The period between 1980 and 1995 is characterized by alternating periods of dominance between state 1 and state 2. For other NAO indices in the literature, this period is

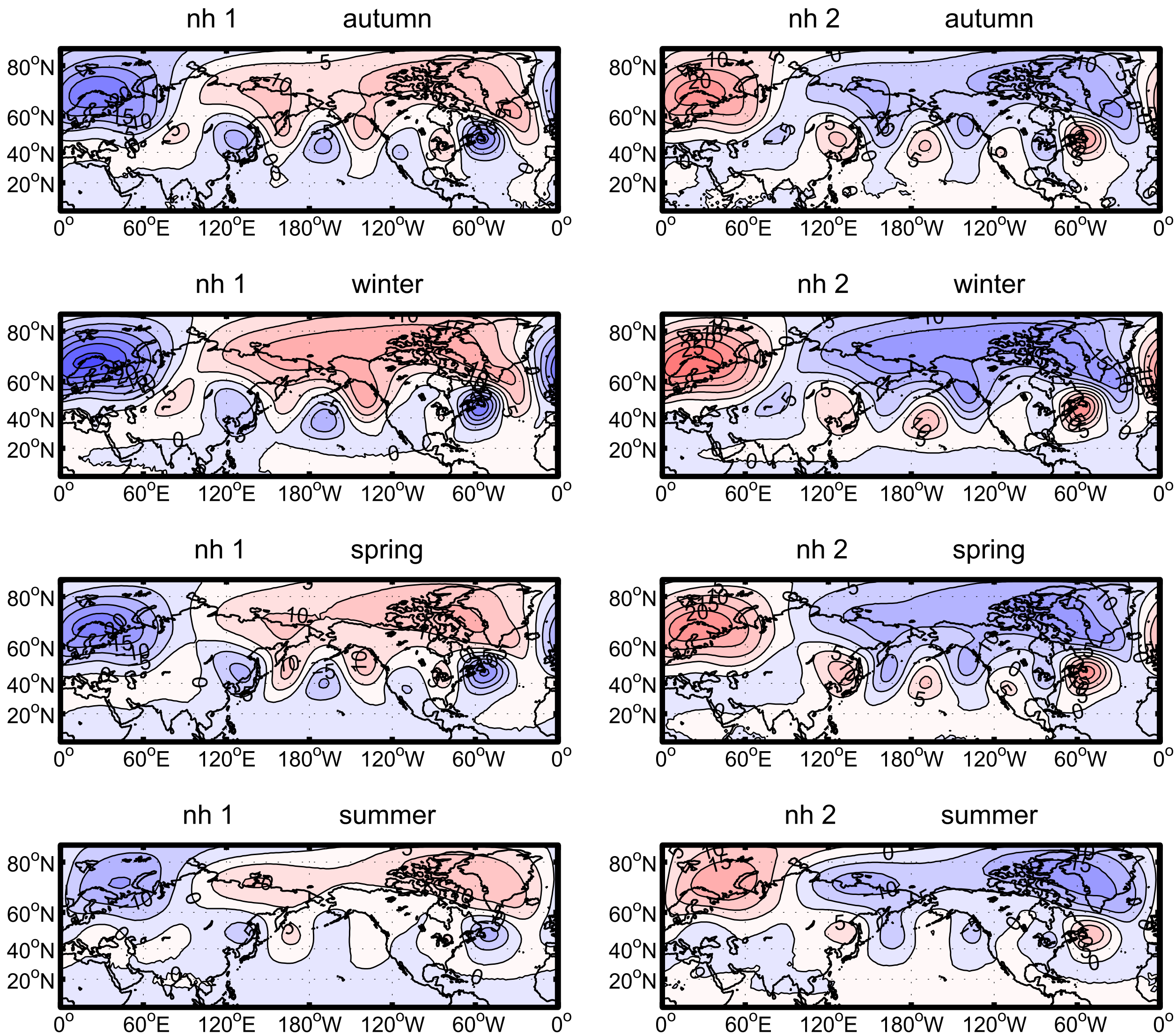

FIG. 9. As in Fig. 6, but for the Northern Hemisphere region for the 20CR 1871–2009 experiment.

characterized as a return to NAO+ dominance (Visbeck et al. 2001), and the NAO index is clearly positive in the annual series in this period (Fig. 10a, bottom panel). In the period since 1995, cluster state 1 is again ascendant, consistent with the return to dominance of NAO− (Halpert and Bell 1997) and the fall in NAO index in Fig. 10a.

b. Pacific

The FEM-BV-VARX cluster state series for the Pacific region is shown in Fig. 10b. The cluster composites in Fig. 3 are a good match with the PNA pattern, so we show the associated PNA index series from NOAA/NCEP at the bottom of Fig. 10b. The two series are moderately well correlated ($r = \pm 0.41$). Cluster state 1 (pac 1) corresponds to negative height anomalies south of the Aleutians (Fig. 3c, left panel) and thus to PNA+. Conversely, cluster state 2 (pac 2) corresponds to PNA−.

The cluster series again exhibits decadal to multidecadal periods where one cluster state dominates the other. From 1955 to 1975, most years are dominated by state 2 (PNA−), with a brief exception around 1960 where state 1 is dominant. The decadal-scale regime flips around 1975 such that cluster state 1 (PNA+) completely dominates from then until about 1989. The next decade then switches to slight dominance by cluster state 2 (PNA−) until 1998. In the period since 1998, the last switch occurs and cluster state 1 (PNA+) is again very dominant. These regimes are broadly consistent with the behavior of the PNA index over these periods (bottom panel), though the PNA index exhibits less apparent regime-like behavior than the cluster states.

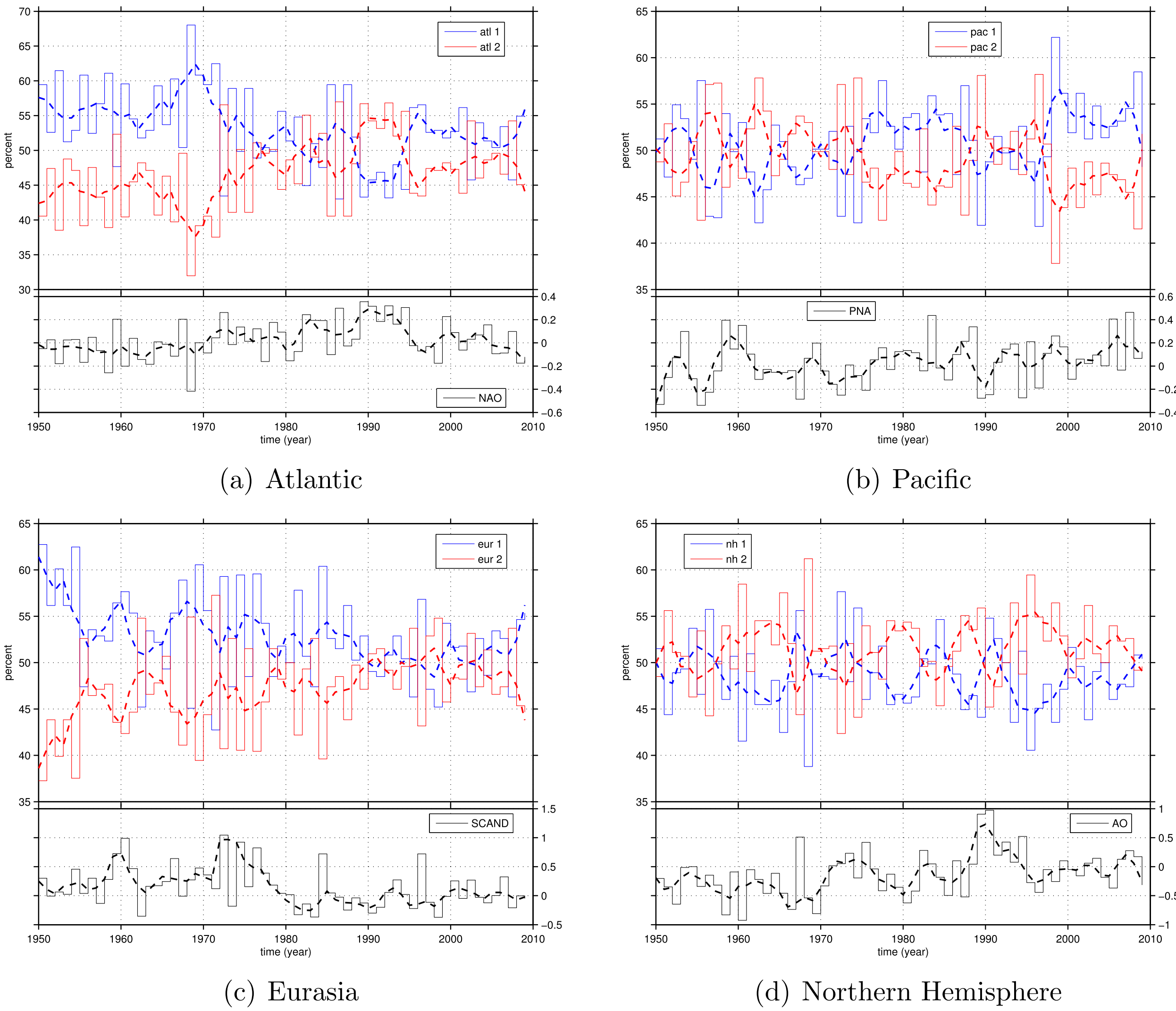

FIG. 10. Time series of FEM-BV-VARX residence percent in state 1 (blue) and state 2 (red) for each year for (a) the Atlantic region, (b) the Pacific region, (c) Eurasia, and (d) the Northern Hemisphere. The FEM-BV-VARX series are for the NNR1 1948–2009 set in (a),(b), and (d) and for 20CR 1948–2009 in (c). For each region, the corresponding NOAA/NCEP teleconnection index is shown (black). The corresponding indices are NAO for the Atlantic region in (a), PNA for the Pacific region in (b), the Scandinavian index for the Eurasia region in (c), and the AO for the Northern Hemisphere in (d). The dashed curve in each case is a loess (Cleveland 1979) smoothed fit to the series.

The regime switches in the cluster state series match well those observed in the literature for the North Pacific region. Shifts in the PDO state in the North Pacific have been documented in 1977 and 1989 (Hare and Mantua 2000) and in 1999 (Bond et al. 2003). These times correspond broadly with the major regime switches observed in the Pacific cluster state.

c. *Eurasia*

The time series of FEM-BV-VARX cluster states for the Eurasian region is shown in Fig. 10c. The composite geopotential patterns for the cluster states for this region in Fig. 4 reflect the Scandinavian blocking pattern. We show the NOAA/NCEP Scandinavian index in the bottom panel of Fig. 10c. The cluster state 1 (eur 1) corresponds to the positive phase of the SCAND pattern (Fig. 4b) with positive height anomalies (blocking) over the Scandinavian region.

The cluster state series shows a strong preference for state 1 (SCAND+) over state 2 in the first four decades until about 1990. Thereafter, the cluster states occur nearly equally often. This preference for strong Scandinavian blocking in the first part of the record and declining blocking thereafter is consistent with the NOAA/NCEP SCAND index, which is strongly positive in the first part of the series and more neutral thereafter. The cluster state and SCAND series are well correlated ($r = \pm0.57$). The strongly positive (high blocking) NOAA/NCEP SCAND years are nearly all reflected as years with a much higher proportion of cluster state 1.

The cluster state series appears to be an appropriate index of blocking in this region and captures years with high blocking activity and longer-period variability in blocking. Since the FEM-BV-VARX method is designed to capture metastable states, and since blocking is a candidate for such a state (Charney and DeVore 1979), the fit is appropriate here. This is also consistent with the demonstrated utility of FEM-BV-VARX for capturing blocking states in the Southern Hemisphere (O'Kane et al. 2013b).

d. Northern Hemisphere

The FEM-BV-VARX cluster state series for the full Northern Hemisphere domain are shown in Fig. 10d. The FEM-BV-VARX composite states for the Northern Hemisphere (Fig. 7) reflect elements of a north–south pressure seesaw (AO) and of a midlatitude circumglobal waveguide (CWP). The waveguide is embedded in the midlatitude portion of the AO (section 3e).

The cluster states (nh 1 and nh 2) in Fig. 10d represent the full AO–CWP structure. There is no other single index of this structure and thus no index directly comparable with the nh 1 and nh 2 cluster series. For a partial comparison, we show an index of the AO from NOAA/NCEP in the bottom panel of Fig. 10d, but this doesn't represent the same structure. This is reflected in the weaker correlation ($r = \pm0.35$) with the cluster state series.

Cluster state 1 (nh 1) features the negative geopotential anomaly in the center of the annulus (Fig. 8b, left panel) and thus maps more closely to AO+. There is some correspondence between the individual year and multiyear peaks in the AO series and cluster state 1, but they do not necessarily have the same long-term behavior. The AO index exhibits a well-known positive trend in the period 1979–90 (Thompson and Wallace 1998; Feldstein 2002), whereas cluster state 1 exhibits strong decadal variability without an obvious trend over this period. The decadal variations in preference for the two waveguide structures provide a source of decadal variability with strong zonal asymmetry in the Northern Hemisphere midlatitude regions.

5. Discussion and conclusions

a. Consistency with conventional methods

The large-scale modes of variability in the Northern Hemisphere have been described in the literature by a number of different approaches. This work extends that by applying a general, nonlinear, nonstationary FEM-BV-VARX model to analysis of these modes. FEM-BV-VARX relaxes some of the assumptions of earlier approaches and still yields structures for the NAO in the Atlantic, the PNA in the Pacific, the Scandinavian block over Eurasia, and the circumglobal waveguide pattern over the Northern Hemisphere, that closely resemble the structures of these modes revealed by prior methods. This is further evidence that these seemingly robust structures are not somehow artefacts of the methods employed. Further, indices of FEM-BV-VARX residence percent and conventional teleconnection indices of these modes show good correlation and similar long-term variability.

b. Reanalysis sensitivity

The FEM-BV-VARX method identifies consistent spatial structures for the teleconnection modes across different reanalysis datasets. The patterns are sometimes more distinct for the longer reanalysis sets tested than for the shorter 1979–2009 sets. While 30 years seems sufficient to generate the teleconnection structures, they are better represented with longer periods. The shorter reanalyses tested (CFSR and NNR1 1979–2009) produce structures consistent with one another.

For the 1948–2009 period, NNR1 and 20CR also produce consistent structures for the different teleconnection modes and regions. This is an important result, in that the 20CR, with only surface observations, is able to generate flow structures for the major teleconnection modes derived from midtropospheric (500 hPa) heights that are consistent with those from NNR1, where upper-air data are included along with surface data. This provides some confidence in interpreting flow structures during earlier periods (prior to 1948) for the 20CR, provided that surface data coverage and quality is not degraded relative to the period after 1948.

The annual time series of residence percent of cluster state for each mode is mostly insensitive to the choice of reanalysis set. For the robust modes (NAO, PNA, and SCAND) where the cluster structures are very similar in the different reanalysis sets, the residence percent time series are also similar across reanalysis experiments. For the CWP–AO mode in the Northern Hemisphere domain, the cluster structures and the residence series are somewhat sensitive to choice of reanalysis experiment.

c. Metastability and regimes

The FEM-BV-VARX method identifies modes of variability as regime transitions between a set of preferred quasi-stationary states. This property means that the method can potentially identify metastable states in atmospheric flow. This work tests whether the major modes of variability identified as teleconnection patterns in the Northern Hemisphere exhibit regime switching characteristic of metastable states. The results suggest that the major teleconnection modes do exhibit this property. Composites of the Viterbi states representing the different regimes yield the canonical structures of these modes as described in the literature.

The "regime" nature of the modes is clearer for the cluster residence series than for conventional continuous indices of the modes. The cluster residence series for each region all display multidecadal variability over the 1950–2009 period. For each mode, there are some decades where one state is favored and other decades where this is reversed. The cluster series in the Atlantic and Pacific regions display regime switches at points in time consistent with documented regime changes in these regions. In the Eurasia region, the cluster state representing Scandinavian blocking captures years with high blocking activity and the enhanced blocking activity observed in other indices in the first half of the period. The depiction of regime states rather than a single index helps to highlight variability in the regimes, and provides a more nuanced view of the flow response than the single index trends.

In each of the domains examined, the optimal number of regime states K was found to equal two. Unlike POP analysis, in which one finds various teleconnections manifesting at different modes, our finding is that for each respective domain, positive and negative phases emerge. In fact, this is what one typically observes in nature and is why many of the empirical indices developed, for example the PNA and NAO, have positive and negative phases.

d. Structures

Some of the major modes of variability revealed in the FEM-BV-VARX composites display latitudinal pressure seesaws (NAO), some exhibit wavelike structures (Scandinavian block), and some appear to combine aspects of both (PNA and the Northern Hemisphere pattern). For example, the PNA structure revealed here has a dominant Aleutian node straddled by a midlatitude wave structure downstream of Asia, spanning the North Pacific. The Atlantic–Eurasia region features a midlatitude waveguide spanning western longitudes. The full Northern Hemisphere domain features an annular structure like the AO but displaced from the pole and where the midlatitude ring is dominated by the CWP waveguide. The wave structures reflect the jet stream waveguide regions and display seasonal movement consistent with the latitudinal changes in waveguide region and changes in spatial scale consistent with seasonal changes in jet intensity.

Established methods for examining the large-scale modes have not proved to be very efficient at revealing waveguide structures. The CWP is a dominant feature of the Northern Hemisphere flow structure and was not well documented until 2002 (Branstator 2002). Established methods can reveal waveguides, but it requires careful selection of variables, levels, and long data samples. Some of the authors of earlier studies pointed to the possibility of combined annular mode and waveguide structures but not as a manifestly evident result of the method. The FEM-BV-VARX method makes no assumptions about the structure of the data and yields both annular modes and waveguide structures. The FEM-BV-VARX method thus provides direct confirmation that the large-scale modes can be viewed as combinations of annular (meridional) modes and waveguide (meridionally trapped) modes.

The FEM-BV-VARX method reveals blocking structures in the blocking regions over Scandinavia and the North Pacific. This is significant in that it provides a measure of blocking that is consistent with one of the dynamical theories of blocking. Some measures of blocking are based on characteristics attributed to blocking such as split flow (Tibaldi and Molteni 1990), but this is not a sufficient condition for blocking (O'Kane et al. 2013b). Charney and DeVore (1979) describe blocking as a quasi-equilibrium process with persistence in a blocked state followed by transitions to a zonal state. That is, blocking is a metastable state with regime transitions. The FEM-BV-VARX method posits this kind of dynamical switching process and reveals spatial blocking structures consistent with those of the predominant blocks in the Northern Hemisphere.

e. Hemispheric comparison

This analysis of major teleconnection modes in the Northern Hemisphere with FEM-BV-VARX provides opportunity for comparison of similar analysis with FEM-BV-VARX in the Southern Hemisphere (O'Kane et al. 2013b). Both hemispheres exhibit annular modes (SAM and NAM/AO) and waveguide structures. The circumglobal waveguide in the Northern Hemisphere has wavenumber 5 [Branstator (2002) and this work], whereas the Southern Hemisphere circumglobal waveguide structure corresponds to wavenumbers 3 and 5 (O'Kane et al. 2013b). The nodes in the Northern Hemisphere waveguide include large dipole structures (PNA and NAO) in the ocean basins, whereas the regional manifestations of the Southern Hemisphere waveguide are monopolar (O'Kane et al. 2013b).

These results and other work suggest that the flow regimes are more "cleanly" separated in the Northern Hemisphere than in the Southern Hemisphere. The evidence for this is in part from barotropic flow models (Zidikheri et al. 2007), which yield very distinct zonal wind velocities in the zonal and blocked states for the Northern Hemisphere (distinct equilibria) and very similar velocities in these two states for the Southern Hemisphere (finely spaced equilibria). Further, the FEM-BV-VARX states are more persistent in the Northern Hemisphere than the Southern Hemisphere. In addition, the spatial structures of the Northern Hemisphere modes are more robust in FEM-BV-VARX and other methods than those of the Southern Hemisphere, which tend to be more sensitive to the method used to elicit them. These results are consistent with the notion that the flow fields in the Southern Hemisphere are less strongly forced (by topography and land–sea contrasts) than in the Northern Hemisphere and, as such, are somewhat more delicately poised to transition between states.

The above hemispheric differences provide insight into the nature of blocking in the respective hemispheres. Blocking tends to occur in the nodes of the circumglobal waveguides. Northern Hemisphere blocks occur in a waveguide mode characterized by persistent states with large dipolar structures in some of the waveguide nodes. Accordingly, Northern Hemisphere blocks often have dipolar structures (Frederiksen 1982) and are long-lived. Southern Hemisphere blocks occur in a waveguide mode that has finely balanced (less persistent) states characterized by monopolar structure in the regional nodes. Southern Hemisphere blocks tend to have monopole structures (O'Kane et al. 2013b), where the blocking high continually breaks down (or progresses) and is replaced in position by another high, rather than having a single high persist in place (Trenberth and Mo 1985). The persistence of the waveguide mode and the form of resonance in its nodes seems to influence the form of blocking. The difference in the respective hemispheric waveguides and regional modes is thus an important reflection of the differences in preferred flow.

Acknowledgments. NCEP reanalysis data were provided by the NOAA/OAR/ESRL PSD in Boulder, Colorado, from their website (http://www.esrl.noaa.gov/psd/). JSR, TJO, and DPM are supported by the Ocean and Climate Dynamics program of CSIRO. TJO is supported by an Australian Research Council Future Fellowship. CF is supported by the Deutsche Forschungsgemeinschaft through the CliSAP Cluster of Excellence. We are grateful for the thorough and constructive reviews of the manuscript.

REFERENCES

Barnston, A. G., and R. E. Livezey, 1987: Classification, seasonality, and persistence of low-frequency atmospheric circulation patterns. *Mon. Wea. Rev.,* **115,** 1083–1126, doi:10.1175/1520-0493(1987)115<1083:CSAPOL>2.0.CO;2.

Bjerknes, J., 1969: Atmospheric teleconnections from the equatorial Pacific. *Mon. Wea. Rev.,* **97,** 163–172, doi:10.1175/1520-0493(1969)097<0163:ATFTEP>2.3.CO;2.

Bond, N., J. Overland, M. Spillane, and P. Stabeno, 2003: Recent shifts in the state of the North Pacific. *Geophys. Res. Lett.,* **30,** 2183, doi:10.1029/2003GL018597.

Bouchet, F., and E. Simonnet, 2009: Random changes of flow topology in two-dimensional and geophysical turbulence. *Phys. Rev. Lett.,* **102,** 094504, doi:10.1103/PhysRevLett.102.094504.

Branstator, G., 2002: Circumglobal teleconnections, the jet stream waveguide, and the North Atlantic Oscillation. *J. Climate,* **15,** 1893–1910, doi:10.1175/1520-0442(2002)015<1893:CTTJSW>2.0.CO;2.

Bueh, C., and H. Nakamura, 2007: Scandinavian pattern and its climatic impact. *Quart. J. Roy. Meteor. Soc.,* **133,** 2117–2131, doi:10.1002/qj.173.

Charney, J. G., and J. G. DeVore, 1979: Multiple flow equilibria in the atmosphere and blocking. *J. Atmos. Sci.,* **36,** 1205–1216, doi:10.1175/1520-0469(1979)036<1205:MFEITA>2.0.CO;2.

Christiansen, B., 2007: Atmospheric circulation regimes: Can cluster analysis provide the number? *J. Climate,* **20,** 2229–2250, doi:10.1175/JCLI4107.1.

Cleveland, W., 1979: Robust locally weighted regression and smoothing scatterplots. *J. Amer. Stat. Assoc.,* **74,** 829–836, doi:10.1080/01621459.1979.10481038.

Compo, G., and Coauthors, 2011: The Twentieth Century Reanalysis project. *Quart. J. Roy. Meteor. Soc.,* **137,** 1–28, doi:10.1002/qj.776.

Corti, S., F. Molteni, and T. Palmer, 1999: Signature of recent climate change in frequencies of natural atmospheric circulation regimes. *Nature,* **398,** 799–802, doi:10.1038/19745.

Ding, Q., B. Wang, J. Wallace, and G. Branstator, 2011: Tropical–extratropical teleconnections in boreal summer: Observed interannual variability. *J. Climate,* **24,** 1878–1896, doi:10.1175/2011JCLI3621.1.

Feldstein, S., 2002: The recent trend and variance increase of the annular mode. *J. Climate,* **15,** 88–94, doi:10.1175/1520-0442(2002)015<0088:TRTAVI>2.0.CO;2.

Franzke, C., and S. Feldstein, 2005: The continuum and dynamics of Northern Hemisphere teleconnection patterns. *J. Atmos. Sci.,* **62,** 3250–3267, doi:10.1175/JAS3536.1.

——, D. Crommelin, A. Fischer, and A. Majda, 2008: A hidden Markov model perspective on regimes and metastability in atmospheric flows. *J. Climate,* **21,** 1740–1757, doi:10.1175/2007JCLI1751.1.

——, I. Horenko, A. Majda, and R. Klein, 2009: Systematic metastable atmospheric regime identification in an AGCM. *J. Atmos. Sci.,* **66,** 1997–2012, doi:10.1175/2009JAS2939.1.

——, T. Woollings, and O. Martius, 2011: Persistent circulation regimes and preferred regime transitions in the North Atlantic. *J. Atmos. Sci.,* **68,** 2809–2825, doi:10.1175/JAS-D-11-046.1.

Frederiksen, J., 1982: A unified three-dimensional instability theory of the onset of blocking and cyclogenesis. *J. Atmos. Sci.,* **39,** 969–982.

——, and P. Webster, 1988: Alternative theories of atmospheric teleconnections and low-frequency fluctuations. *Rev. Geophys.,* **26,** 459–494, doi:10.1029/RG026i003p00459.

——, and G. Branstator, 2001: Seasonal and intraseasonal variability of large-scale barotropic modes. *J. Atmos. Sci.,* **58,** 50–69, doi:10.1175/1520-0469(2001)058<0050:SAIVOL>2.0.CO;2.

Halpert, M., and G. Bell, 1997: Climate assessment for 1996. *Bull. Amer. Meteor. Soc.,* **78,** S1–S49, doi:10.1175/1520-0477(1997)078<1038:CAF>2.0.CO;2.

Hare, S., and N. Mantua, 2000: Empirical evidence for North Pacific regime shifts in 1977 and 1989. *Prog. Oceanogr.,* **47,** 103–145, doi:10.1016/S0079-6611(00)00033-1.

Horenko, I., 2010a: On clustering of non-stationary meteorological time series. *Dyn. Atmos. Oceans,* **49,** 164–187, doi:10.1016/j.dynatmoce.2009.04.003.

——, 2010b: On the identification of nonstationary factor models and their application to atmospheric data analysis. *J. Atmos. Sci.,* **67,** 1559–1574, doi:10.1175/2010JAS3271.1.

——, 2011: On analysis of nonstationary categorical data time series: Dynamical dimension reduction, model selection, and applications to computational sociology. *Multiscale Model. Simul.,* **9,** 1700–1726, doi:10.1137/100790549.

Hurrell, J. W., 1995: Decadal trends in the North Atlantic Oscillation: Regional temperatures and precipitation. *Science,* **269,** 676–679, doi:10.1126/science.269.5224.676.

——, and C. Deser, 2009: North Atlantic climate variability: The role of the North Atlantic Oscillation. *J. Mar. Syst.,* **78,** 28–41, doi:10.1016/j.jmarsys.2008.11.026.

Kalnay, E., and Coauthors, 1996: The NCEP/NCAR 40-Year Reanalysis Project. *Bull. Amer. Meteor. Soc.,* **77,** 437–471, doi:10.1175/1520-0477(1996)077<0437:TNYRP>2.0.CO;2.

Kimoto, M., and M. Ghil, 1993: Multiple flow regimes in the Nothern Hemisphere winter. Part I: Methodology and hemispheric regimes. *J. Atmos. Sci.,* **50,** 2625–2643, doi:10.1175/1520-0469(1993)050<2625:MFRITN>2.0.CO;2.

Lorenz, E., 1951: Seasonal and irregular variations of the Northern Hemisphere sea-level pressure profile. *J. Meteor.,* **8,** 52–59, doi:10.1175/1520-0469(1951)008<0052:SAIVOT>2.0.CO;2.

Majda, A., C. Franzke, A. Fischer, and D. Crommelin, 2006: Distinct metastable atmospheric regimes despite nearly Gaussian statistics: A paradigm model. *Proc. Natl. Acad. Sci. USA,* **103,** 8309–8314, doi:10.1073/pnas.0602641103.

Metzner, P., L. Putzig, and I. Horenko, 2012: Analysis of persistent nonstationary time series and applications. *Commun. Appl. Math. Comput. Sci.,* **7,** 175–229, doi:10.2140/camcos.2012.7.175.

Michelangeli, P., R. Vautard, and B. Legras, 1995: Weather regimes: Recurrence and quasi stationarity. *J. Atmos. Sci.,* **52,** 1237–1256, doi:10.1175/1520-0469(1995)052<1237:WRRAQS>2.0.CO;2.

Mo, K., and R. Livezey, 1986: Tropical–extratropical geopotential height teleconnections during the Northern Hemisphere winter. *Mon. Wea. Rev.,* **114,** 2488–2515, doi:10.1175/1520-0493(1986)114<2488:TEGHTD>2.0.CO;2.

O'Kane, T., R. Matear, M. Chamberlain, J. Risbey, B. Sloyan, and I. Horenko, 2013a: Decadal variability in an OGCM Southern Ocean: Intrinsic modes, forced modes and metastable states. *Ocean Modell.,* **69,** 1–21, doi:10.1016/j.ocemod.2013.04.009.

——, J. Risbey, C. Franzke, I. Horenko, and D. Monselesan, 2013b: Changes in the metastability of the midlatitude Southern Hemisphere circulation and the utility of nonstationary cluster analysis and split-flow blocking indices as diagnostic tools. *J. Atmos. Sci.,* **70,** 824–842, doi:10.1175/JAS-D-12-028.1.

Saha, S., and Coauthors, 2010: The NCEP Climate Forecast System Reanalysis. *Bull. Amer. Meteor. Soc.,* **91,** 1015–1057, doi:10.1175/2010BAMS3001.1.

Thompson, D., and J. Wallace, 1998: The Arctic Oscillation signature in the wintertime geopotential height and temperature fields. *Geophys. Res. Lett.,* **25,** 1297–1300, doi:10.1029/98GL00950.

Tibaldi, S., and F. Molteni, 1990: On the operational predictability of blocking. *Tellus,* **42A,** 343–365, doi:10.1034/j.1600-0870.1990.t01-2-00003.x.

Trenberth, K., and K. Mo, 1985: Blocking in the Southern Hemisphere. *Mon. Wea. Rev.,* **113,** 3–21, doi:10.1175/1520-0493(1985)113<0003:BITSH>2.0.CO;2.

Van den Dool, H., S. Saha, and A. Johansson, 2000: Empirical orthogonal teleconnections. *J. Climate,* **13,** 1421–1435, doi:10.1175/1520-0442(2000)013<1421:EOT>2.0.CO;2.

Visbeck, M., J. Hurrell, L. Polvani, and H. Cullen, 2001: The North Atlantic Oscillation: Past, present, and future. *Proc. Natl. Acad. Sci. USA,* **98,** 12 876–12 877, doi:10.1073/pnas.231391598.

von Storch, H., G. Bürger, R. Schnur, and J. von Storch, 1995: Principal oscillation patterns: A review. *J. Climate,* **8,** 377–400, doi:10.1175/1520-0442(1995)008<0377:POPAR>2.0.CO;2.

Wallace, J. M., and D. S. Gutzler, 1981: Teleconnections in the geopotential height field during the Northern Hemisphere winter. *Mon. Wea. Rev.,* **109,** 784–812, doi:10.1175/1520-0493(1981)109<0784:TITGHF>2.0.CO;2.

Zidikheri, M., J. Frederiksen, and T. O'Kane, 2007: Multiple equilibria and atmospheric blocking. *Frontiers in Turbulence and Coherent Structures,* J. Denier, Ed., World Scientific Lecture Notes in Complex Systems, Vol. 6, World Scientific, 59–85.